

Ground-Penetrating Radar (GPR) imaging of near-surface structure in a carbonate environment

Julie A. Aitken and Robert R. Stewart

ABSTRACT

Since 2001, a number of ground-penetrating radar (GPR) surveys, and near-surface seismic surveys have been conducted at the ancient Maya site of Ma'ax Na in Belize, Central America. The surveys were initiated to assist archaeologists in focusing their excavation activities.

The Ma'ax Na project involved the surveying of several sites within the complex including the plaza and several caves. GPR acquisition consisted of several orthogonal 2-D lines, and two 3-D grids. The report will deal with the GPR records of the plaza only.

This research project has focussed on improving the quality of the GPR images generated from the Ma'ax Na plaza lines, and has attempted to interpret these images based on the archaeological information. In doing so, a more definitive processing and interpretation flow has been established.

The survey was acquired using Sensors and Software's Noggin® and Smart Cart® System, at a GPR antennae frequency of 250 MHz. Spatial sampling of 5 centimetres and a temporal sampling of 0.04 nanoseconds provided reasonable quality records, with good signal penetration. The maximum penetration depth of the plaza lines was about 1.8 m. The recorded velocities in 2002 ranged from 0.106 m/ns @ 0.7 m and 0.072 m/ns @ 1m and were calculated from the hyperbolic fitting of curves to point diffractors. In 2003, the measured velocities were noticeably higher in the range of 0.122 to 0.140 m/ns. We attribute this increase due to very dry conditions in the area compared to the year before.

Resolution based on a velocity of 0.072m/ns and the antennae frequency of 250 MHz was approximately 7.2 cm. Excellent ties between intersecting plaza lines and the duplicity between two lines shot in reverse directions inspired confidence in the accuracy of the acquisition. Modelling of the GPR based on changes in the electrical properties of dielectric permittivity revealed a reasonable correlation between the synthetic radargram and the GPR image. Surficial discontinuities (roots) and anomalous buried features were identified.

INTRODUCTION

Ma'ax Na is one of a number of Maya sites in the Rio Bravo Conservation area of Belize (Figure 1). This area is dedicated to the preservation of archaeological sites and the wildlife that reside there. The Ma'ax Na site was discovered in 1995 by surveyors. The subsequent excavation has revealed more than 25 intact structures. These ancient landmarks, buried within the jungles of Belize, provide archaeologists with the necessary cultural footprints to assist in unraveling and reconstructing the history of the Maya.

Research at the University of Calgary has attempted to not only identify buried artifacts and structures but to improve the geophysical records through enhanced processing techniques and improved acquisition parameters (Fisher et al., 1996).

This paper will focus specifically on fine-tuning the sequence of processing steps, attempting to model the excavated pit, documenting an interpretation procedure, and identifying anomalous features within the plaza floor.

REGIONAL AND STRATIGRAPHIC SETTING

Belize is located in northeastern Central America and is bounded by Mexico, Guatemala, and the Caribbean Sea. It has an areal extent of 22,700 square kilometers and is the only Central American country with no Pacific coastline (Aitken, 2002).

Continental drift of the North American plate precipitated the formation of new oceanic crust in an area adjacent to Belize, forming the Caribbean plate. Continued tectonic activity led to the eastward movement of the Caribbean plate which deformed the Central American region, and is responsible for the dominant and structurally controlled features of Belize today: the Maya Mountains, the offshore atolls and the coral barrier reefs (Geology and Petroleum Office, 1995).

The Belize mainland can be subdivided into three geological provinces: Northern Belize, Southern Belize and South-Central Belize. The Corozal Basin of Northern Belize is an extension of the Yucatan platform and is stratigraphically part of the North Peten Basin of Guatemala. Southern Belize contains the Belize basin, and the Maya Mountains are part of the South-Central Belize geological province. This report will focus on the Corozal Basin.

The Ma'ax Na site is located in the Corozal Basin, and is comprised of a thick sequence of marine carbonates deposited during a 50 million year history of tectonic uplift, erosion, faulting and transgressions. The geography of the Three Rivers region consists of a series of escarpments formed by faulting, slumping and weathering. Gentle topography, low lying plains and lakes formed by subterranean karsting characterize the region (Aitken, 2002).

THE MAYA CULTURE

The Maya civilization flourished in Central America culminating in what is known as the Classic Period (A.D. 300-900). Monumental architecture in the form of pyramids, temples, stelae and plazas, were erected within great cities, to pay homage to the gods and rulers, and bring balance to the cosmos (Wenke, 1999). Figure 2 represents a layout of the great Maya city of Copan. Although Ma'ax Na was on a much smaller scale, Maya architecture and complexes were similar throughout Central America. Great plaza areas linked various pyramids and structures, and were interspersed with stelae (tall columnar stone monuments). The Maya believed the sky was one of three plains of existence within the universe. Mountain peaks were considered to be connection points to the cosmos, where deities and ancestors resided. Pyramids and any elevated structures were considered to be energy centres. Thus, the Maya rarely leveled anything choosing to

expand upward and outward. In fact, Maya architecture accommodated local topography and many of its massive structures are built on limestone outcrops of Early Tertiary age (Miller, 1999).

The near surface is comprised mainly of soil, with assorted limestone detrital material above limestone bedrock. The Maya used the resources available to them so construction materials included soil, limestone cobbles and boulders, large crudely chiseled limestone blocks, and stucco (Wilson and Wilson, 1990). They also determined that if the limestone fragments were burned and the resulting powder mixed with water, a white plaster of great durability was obtained (Coe, 1975). This plaster was then used for the surface of the plazas and to coat the numerous temples and pyramid structures.

GPR SURVEY

Ground penetrating radar (GPR) involves the propagation of a series of short pulses of electromagnetic energy into the subsurface. In terms of an archaeological context, the transmitted signal travels through the lithologic layers of the earth, scattering and reflecting off stratigraphic boundaries, walls, house floors, pits or rubble (Goldberg, 2001). The resultant GPR image represents a series of reflections or events which constitute changes in the impedance of one or more of its electrical properties. The recorded signal is generally measured in nanoseconds.

Ground penetrating radar operates in the frequency range of 1-1000MHz, known as the GPR plateau, where velocity and attenuation are considered independent of frequency. The success of GPR surveys is also site dependent. The composition of near surface materials and conditions, such as the clay content of soils and the saturation level of the material, all play key roles in obtaining interpretable images of the earth.

As shown in Figure 3, several 2-D lines and 3-D grids have been surveyed on the Ma'ax Na plaza over the last several years. The method employed for the 3-D acquisition is termed forward-reverse, and is outlined in Figure 4. This involves obtaining every second line in the reverse direction to make the most efficient use of acquisition time. The GPR survey equipment consisted of a Noggin® 250 and Smart Cart® system manufactured by Sensors and Software Inc. This represents a monostatic system in which the transmitter and receiver antennae are housed in the same unit at a fixed interval of 27.94 cm. The frequency employed was a 250 MHz antenna with an associated bandwidth of 125-375MHz (Moldoveanu, 2002). Spatial sampling (station interval) was set at 5 centimetres with temporal sampling (sample rate) at 0.4 nanoseconds. A listing of the acquisition parameters is outlined in Tables 1.

PHYSICAL PROPERTIES AND MODELLING

The aim of geophysical surveying is to measure contrasts in the physical properties of the subsurface to deduce information about the composition and distribution of near surface materials. As ground-penetrating radar is a geophysical tool employing electromagnetic waves, understanding the behavior of electrical and magnetic fields, and the properties of matter is a necessary first step in resolving a correct and meaningful

interpretation (Olehoft, 2000). The physical properties that affect radar waves are the dielectric permittivity, electrical conductivity and the magnetic permeability.

Electrical polarization, or dielectric permittivity, is the motion of subatomic particles from neutral equilibrium positions to displaced, non-neutral positions under the effect of an applied electromagnetic field (Nabighian, 1998). The dielectric permittivity of a medium can vary with saturation, composition, type of pore fluid, material texture, and temperature (Hubbard, 1997). Table 2 contains a list of the dielectric permittivities of common rocks and near surface materials.

Magnetic polarization (permeability or susceptibility) is created by the rotation and motion of electrons in atomic orbits (Olehoft, 2003). The magnetic properties of most geologic materials, barring those rocks that contain high concentrations of magnetic minerals, are considered to be similar to those of a vacuum. Therefore it is relatively common to make the assumption that the magnetic permeability is equal to one.

At the high frequencies employed during GPR data acquisition, and assuming the surface is non-magnetic and contains low-loss (non-conductive) materials, the velocity of radar waves in a medium is given by the following formula (Conyers and Goodman, 1997):

$$V = \frac{c}{(\epsilon_r)^{\frac{1}{2}}} = \frac{0.3}{(\epsilon_r)^{\frac{1}{2}}} \text{ m/ns.} \quad (1)$$

where V = average velocity of the radar pulse,

ϵ_r = relative dielectric constant (RDP)

c = .3m/ns (speed of light).

Conversely, this formula may be written as

$$\epsilon_r = RDP = \frac{c^2}{V^2} = \frac{0.09}{V^2} \quad (2)$$

The relative dielectric permittivity (RDP) of a material is its capacity to store and allow the motion of charges within an imposed electromagnetic field. It is dimensionless. RDP is calculated as the ratio of a material's electrical permittivity to the electrical permittivity of a vacuum, which has an RDP of 1 (Conyers and Goodman, 1997).

Amplitudes of the reflections generated on a GPR profile, are the direct result of the differences between the relative dielectric permittivities of materials within the subsurface. The magnitude of the reflection generated at the interface can be shown as (Conyers and Goodman, 1997):

$$R = \frac{[\sqrt{(\epsilon_{r1})} - \sqrt{(\epsilon_{r2})}]}{[\sqrt{(\epsilon_{r1})} + \sqrt{(\epsilon_{r2})}]} \quad (3)$$

where R = coefficient of reflectivity at a buried surface

ϵ_{r1} = RDP of overlying material

ϵ_{r2} = RDP of underlying material.

Significant reflections are generated when changes in the dielectric permittivity between two materials occur over a small distance. When the RDP changes gradually with depth, only minute differences in reflectivity will occur, resulting in the absence of a reflector or at best a weak response (Conyers and Goodman, 1997).

The wavelength of the GPR pulse is calculated using the following formula:

$$\lambda = \frac{V}{f} \quad (4)$$

Incorporating a frequency of 250 MHz and an average velocity of 0.072 m/ns, the wavelength was 28.8 centimetres. Assuming a vertical resolution of $\lambda/4$, the resolution is given as 7.2 centimetres.

In 2003, the measured velocities were noticeably higher in the range of 0.122 to 0.140 m/ns. We attribute this increase to drought conditions in the area.

PROCESSING

In collaboration with GEO•X Systems Ltd. in Calgary, the GPR processing sequence was refined based on testing of deconvolution, scaling, and migration algorithms. As the system is geared toward seismic processing, additional formatting and resampling steps were required (Aitken, 2002).

The following assumptions have been made to process the GPR data:

1 ns GPR = 10 ms seismic, therefore 100 ns GPR = 1 s seismic

Velocities: The average velocity as determined from point diffractors: 0.072 m/ns

Therefore, 0.072 m/ns x 100 ns/s = 7.2 m/s

Frequencies: The bandwidth of the GPR data is 125 – 375 MHz.

Therefore, 125 x 10⁶ cycles/s x 1s/ 10⁹ ns = 0.125 cycles/ns

If 1s = 100 ns, then it follows that 0.125 cycles/ns x 100 ns/s = 12.5 Hz

0.375 cycles/ns x 100 ns/s = 37.5 Hz

All of the GPR records are posted in milliseconds (ms).

The processing steps are outlined in Figure 5. The flow consisted of reformatting and resampling steps to convert the data to a seismic based system, the application of automatic gain control (AGC) with a 60 ms operator, a debias window the length of the trace, a bulk shift (to bring the airwave to time zero) of 160 ms, a selective smoothing AGC with a 60 ms operator, a predictive deconvolution filter with a 50 ms operator and a 30 ms lag, finite difference migration incorporating an interval velocity of .106 m/ns @ 1m and 0.041 m/ns for data below 1m, and a final recursive Butterworth filter of 8-42 Hz.

Choosing the ideal decon parameters was a daunting task at best since it was difficult to determine what events were “real” on the GPR sections acquired at the plaza. In an attempt to capture a more realistic surface signature, a rebar experiment was conducted on the plaza. The rebar was pounded into one of the sides of the unearthed excavated pit at a depth of 0.76 m. A series of GPR lines were then acquired directly over the rebar. Figure 6 is an example of one of these lines. Future work will include trying to obtain the true wavelet signature, by windowing, flattening and stacking the hyperbola associated with the rebar’s point diffractor.

The convolution of the transmitted wavelet with the earth’s near surface results in the GPR image. If we could successfully identify the shape of this wavelet, and extract or deconvolve it through the use of an inverse filter, the resultant image should be a “true” picture of the subsurface. The deconvolution process attempts to do this, but with limited knowledge of the composition of the plaza, determining whether the standard decon testing is doing a correct job is guesswork.

MODELLING

A recent excavation of a one-by-one meter pit at the plaza revealed detailed information about its composition (left side of Figure 7). At least seven previous levels of plaza construction were evident interspersed with rubble and cobble layering. Based on the theoretical resolution of the GPR data as calculated above, it may be possible to identify some of these levels. Rubble zones provide permeable horizontal pathways and are considered to be major conduits for fluid flow (Hubbard, et al, 1997). The electromagnetic properties of common earth materials can vary radically and randomly over small distances. Large property changes may be created by water saturation. For example, dielectric constants may increase up to 20% with the infiltration of fluid along a preferential flow path (Hubbard, et al, 1997).

With this in mind, modelling of the GPR response was generated through SYNTH, a seismic based modeling package. Seismic modeling is based on changes in acoustic impedance, which is the product of seismic velocity and density. The seismic velocity or slowness log was replaced by a constant background radar velocity of 0.072 m/ns (converted to a pseudo slowness log), and the density log was manipulated to represent the dielectric permittivity log. The pseudo-dielectric permittivity log was created by increasing the dielectric permittivity values by 20% over those areas in the excavated pit that contained rubble or small rocks. The logs were then convolved with a 250Hz minimum phase wavelet. The resultant GPR synthetic is aligned with the archaeological

information, the pseudo-radar slowness log (blue) and the pseudo-dielectric permittivity log (red) for comparison (Figure 7).

INTERPRETATION

The first two major events on GPR sections are the airwave and the ground wave. The velocity of the airwave is close to the speed of light at 0.3 m/ns. The ground wave is much slower with a velocity of 0.1m/ns. All subsequent events are considered to be subsurface information. Unlike seismic propagation, radar velocities generally decrease with depth.

Present-day plaza levels can often overlie other levels of plaza, tombs, caches and even drainage systems (pers. comm., Shaw, 2002). When interpreting the sections, one looks for discontinuities in the events or apparent amplitude variations. Buried objects are often located by the presence of point diffractors, which result in flattened hyperbolic patterns of energy. The surrounding material is often disturbed and the continuity of the geological layering is compromised.

Figure 8 shows the excellent ties between two intersecting GPR lines. The next two displays (Figures 9 and 10), represent a comparison between two lines shot in identical positions but in reverse directions on the plaza. These sections serve to validate the integrity of the GPR data and repeatability of the acquisition method.

The interpretation process we have employed with the GPR sections is one which the typical seismic interpreter would use in trying to interpret seismic data. The first task is to gain an understanding of the rocks and geology in the particular play one is pursuing. Next, the geophysicist would study nearby pools for an analogy to that particular play type or look at any logs available in the area and model the seismic response that would be expected through manipulation of the logs to the geologic scenario. The last stage would be to compare the seismic response or synthetic to the data to look for similar features and to determine the correct placement of geologic horizons.

Based on the GPR synthetic, or radargram, it was possible to make an initial interpretation of the filtered, deconvolved and migrated N-S Plaza Line 2 (Figure 11). The radargram, based on the archaeological information from the excavated pit, ties fairly well with the GPR image. Individual layers (lots) could be assigned a position on the GPR section (peak, trough or zero crossing). The interpreted section represents the part of the line closest to the excavated pit. The lot numbers have been color coded to help distinguish the various levels and to help focus the eye on the lateral continuity of the events (Figure 12). Choppiness of the events is expected, and the direct result of the electromagnetic energy being scattered off the cobbles and rubble which constitute many of the layers.

Figures 13-15 show the processed sections and the anomalies associated with them. Red circles identify anomalies on the various lines. In some cases, buried roots and cobbles did appear to cause interference between events. A metal pin at trace 1000 on the N-S Plaza Line 2 was also detected.

The remaining figures are the most recent sections obtained from the 3-D surveys. The raw records in Figure 16 serve to demonstrate the location of the excavated pit after it had been refilled, as imaged by discontinuous and weak reflections. The amplitude slices through the data volume, (Figure 17), indicate average amplitude variations at depth intervals of 0.76m, and the 3-D data cubes (Figures 18 and 19), show a similar anomalous feature at 33.7 ms in both the X (in-line) and Y (cross-line) directions. Note the loss in resolution in the direction of interpolation.

Future work will involve merging the two data volumes and interpretation using 3-D interpretation software.

The results of the final interpretation and the cataloguing of interesting anomalies found on the various surveys will be forwarded to the archaeologists at Ma'ax Na. The 2004 archaeological field season in Belize may result in the excavation of these anomalous features for possible buried artifacts of the Maya.

We, as earth scientists, must be cognizant of the fact that these areas are sacred and ceremonial sites of our ancient peoples. We are indeed privileged to be a part of the exploration of human history.

CONCLUSIONS

The GPR method provides coherent and interpretable images of the near surface structure of the plaza. The GPR lines have highlighted a number of interesting features which may be helpful to the archaeologists studying and excavating at Ma'ax Na.

The depth of penetration is about 1.8 m, and the theoretical vertical resolution is approximately 7.2 cm. We interpret the resolution to be approximately 10 cm from the sections.

We have established an improved processing flow using various scaling, deconvolution and migration algorithms.

We have developed an interpretation procedure similar to that employed by exploration seismologists to help identify subsurface horizons.

ACKNOWLEDGEMENTS

The authors wish to acknowledge the support of members of the CREWES Project especially Kevin Hall and Peter Manning; Laurie Ross and Mike Perz at GEO•X Systems Ltd., expertly assisted in processing the data and Leslie Shaw and Claire Allum of Bowdoin College, Brunswick, Maine, and Eleanor King of Howard University, Washington, D.C. have ably assisted in acquiring the data, arranging logistics and permits, and in the understanding of the archaeological setting at Ma'ax Na.

REFERENCES

- Aitken, J.A., 2002, A geological/geoscience overview of the hydrocarbon potential of Belize, Central America: CREWES Research Report, **14**.
- Baker, G.S., Steeples, D.W., and Schmeissner, C., 1999, SEG Expanded Abstracts.
- Coe, M. C., 1975, *The Maya*: 236 p.
- Conyers, L.B., and Goodman D., 1997, Ground penetrating radar- an introduction for archaeologists: 232 p.
- Cubola Productions, 1997, A geography of Belize: 139 p.
- Davis, J.L., and Annan, A.P., 1989, Ground penetrating radar for high resolution mapping of soil and rock stratigraphy: *Geophysical Prospecting*, **37**, p. 531-551.
- Fisher, E., McMechan, G.A., Annan, A.P., and Cosway, S.W., 1992, Examples of reverse-time migration of single channel ground penetrating radar profiles: *Geophysics*, **57**, p. 577-586.
- Fisher, E., McMechan, G.A., and Annan, A.P., 1992, Acquisition and processing of wide-aperture ground penetrating radar data: *Geophysics*, **57**, p. 495-504.
- Fisher, S.C., Stewart, R.R, and Jol, H., 1996, Ground penetrating radar (GPR) data enhancement using seismic techniques, *Journal of Environment, Engineering and Geophysics*, **1**, p. 89-96.
- Goodman, D., 1994, Ground-penetrating radar simulation in engineering and archaeology: *Geophysics*, **59**, p. 224-232.
- Goldberg, P., 2001, *Earth Sciences and Archaeology*: 513 p.
- Henley, D.C., 2002, Near surface imaging: refraction tomography and reflection imaging: CREWES Research Report, **14**.
- Hubbard, S.S., Petersen, J.E., et al, 1997, Estimation of permeable pathways and water content using tomographic radar data: *The Leading Edge*, **16**, p. 1623-1628.
- Jol, H.M., and Dechaine, R.J., 2002, Archaeological GPR Investigation at Rennes-Le-Chateau, France, University of Wisconsin-Eau Claire.
- Jol, H.M., 2002, GPR investigations at Qumran, Israel: Site of the Dead Sea scroll discovery, Ninth International Conference on Ground Penetrating Radar, **2758**: p. 125-129.
- Keller, G.V., and Frischknecht, F.C., 1979, *Electrical Methods in Geophysical Prospecting*, Pergamon of Canada, Willowdale, Ontario, p. 1-60.
- Knight, R., and Tercier, P., 1997, The role of ground-penetrating radar and geostatistics in reservoir description: *The Leading Edge*, **16**, p. 1576-1582.
- Miller, M. E., 1999, *Maya art and architecture*: 240 p.
- Moldoveanu, M., Stewart, R.R, and Aitken, J.A., 2002, Shallow imaging using ground penetrating radar (GPR) data in a carbonate environment in Belize, Central America: CREWES Research Report, **14**.
- Nabighian, 1998 *Electromagnetic Methods*
- National Geographic, 1989, *City of kings and commoners – Copan*: Vol. 176, p.494.
- Olehoft, G.R., 2000, Maximizing the information return from ground penetrating radar: *Journal of Applied Geophysics*, **43**, p. 175-187.
- Powers, M., 1997, Modeling frequency-dependent GPR: *The Leading Edge*, **16**, p. 1657-1662.
- Reynolds, J.M., 1997, *An introduction to applied and environmental geophysics*: John Wiley & Sons, New York.
- Shaw, L., 2002, Personal communication, Dept. of Sociology and Anthropology, Bowdoin College, Maine.
- Shen, L.C., Savre, W.C., Price, J.M., and Athavale, K., 1985, Dielectric properties of reservoir rocks at ultra-high frequencies: *Geophysics*, **50**, p. 692-704.
- The Ma'ax Na Archaeology Project, 2001, <http://www.neararchaeology.or/project>.
- Wenke, Robert J., 1999, *Patterns in prehistory*: Oxford University Press, New York.
- Wilson, W.L. and Wilson, D.C., 1990, Investigation of Mayan structures at Caracol, Belize, using ground penetrating radar: Third International Conference of Ground Penetrating Radar, U.S Geological Survey, Open-File Report 90-414, p. 74.

Table 1 Acquisition parameters for Plaza lines

GPR Acquisition Parameters	2002 2-D data		2003 2-D Data		
	Line 1	Line 2	Line 3	Rebar line	Plaza length
# of Traces	990	1874	786	44	1360
Station interval (cm)	5	5	5	5	5
Sample rate (ns)	0.4	0.4	0.4	0.4	0.4
Length of line (m)	49.45	93.65	39.25	2.2	68
Nominal Frequency (MHz)	250	250	250	250	250
Antenna Separation (cm)	27.94	27.94	27.94	27.94	27.94

Table 2 Dielectric permittivity for common near surface materials (modified from Hubbard et al, 1997).

Material	Dielectric Constant	Radar Velocities m/ns
Sand (dry)	3-6	.173 - .100
Sand (saturated)	20-30	.067 - .055
Silts	5-30	.134 - .055
Shales	5-15	.134 - .078
Clays	5-40	.134 - .047
Humid soil	30	.055
Cultivated soil	15	.078
Rocky soil	7	.113
Sandy soil (dry)	3	.173
Sandy soil (saturated)	19	.069
Clayey soil (dry)	2	.212
Clayey soil (saturated)	15	.078
Sandstone (saturated)	6	.100
Limestone (dry)	7	.113
Limestone (saturated)	4-8	.150 - .106
Basalt (saturated)	8	.106
Granite (dry)	5	.134
Granite (saturated)	7	.113



FIG. 1 Location of the Maya site of Ma'ax Na in Belize, Central America (The Ma'ax Na Archaeology Project, 2001).

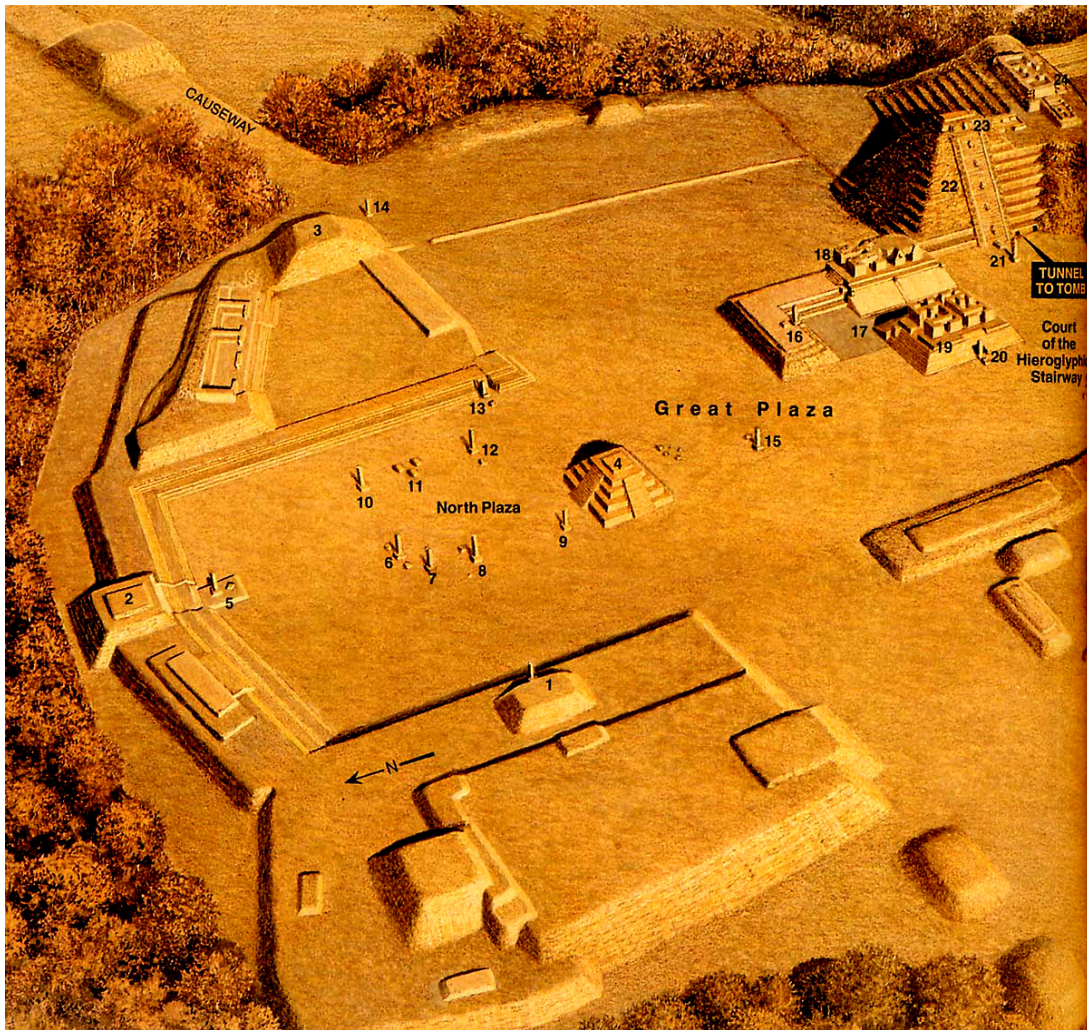


FIG. 2. The layout of a portion of the Maya city of Copan. Note the size of the plazas which connect the causeways and various structures within the city. The numbers represent specific features such as the pyramids, temples, stelae and hieroglyphic staircases (National Geographic, 1989).

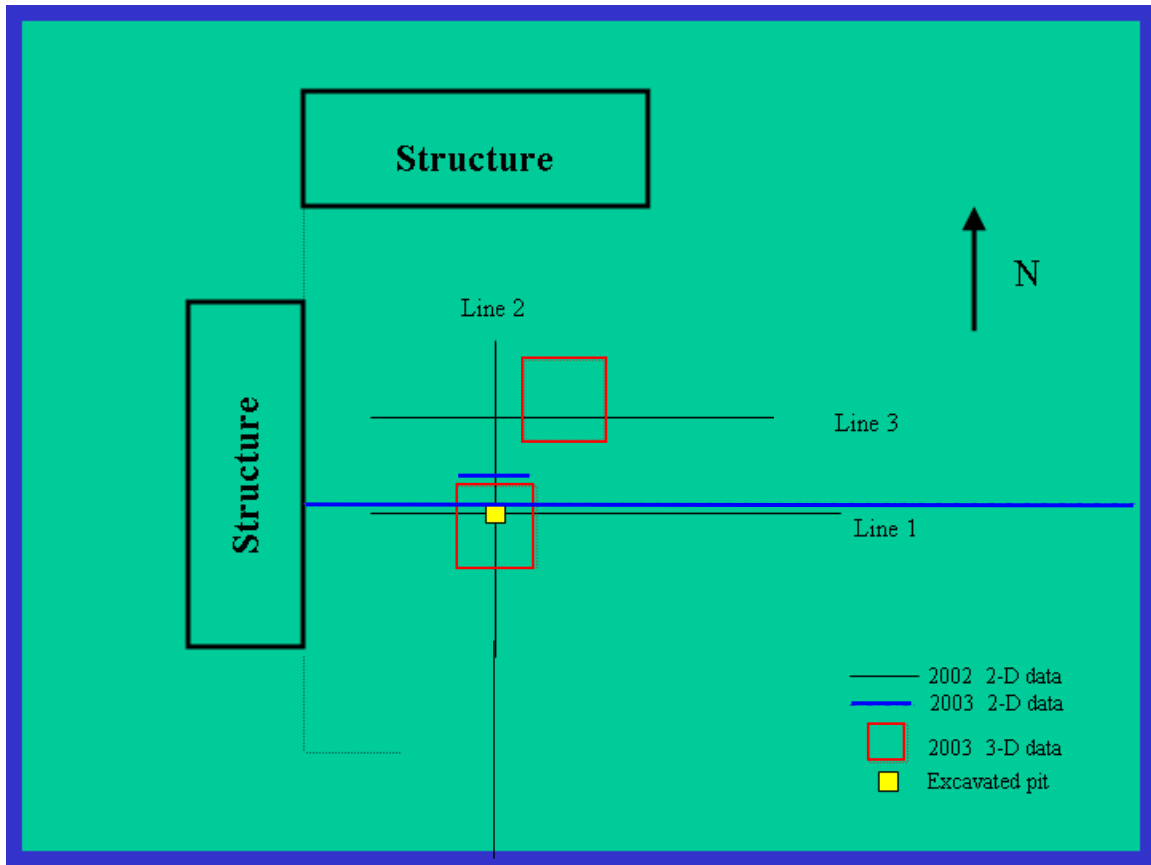


FIG. 3 Layout of GPR lines at the Ma'ax Na plaza complex for the 2002 and 2003 field seasons. Note the excavated pit and line dimensions are approximate.

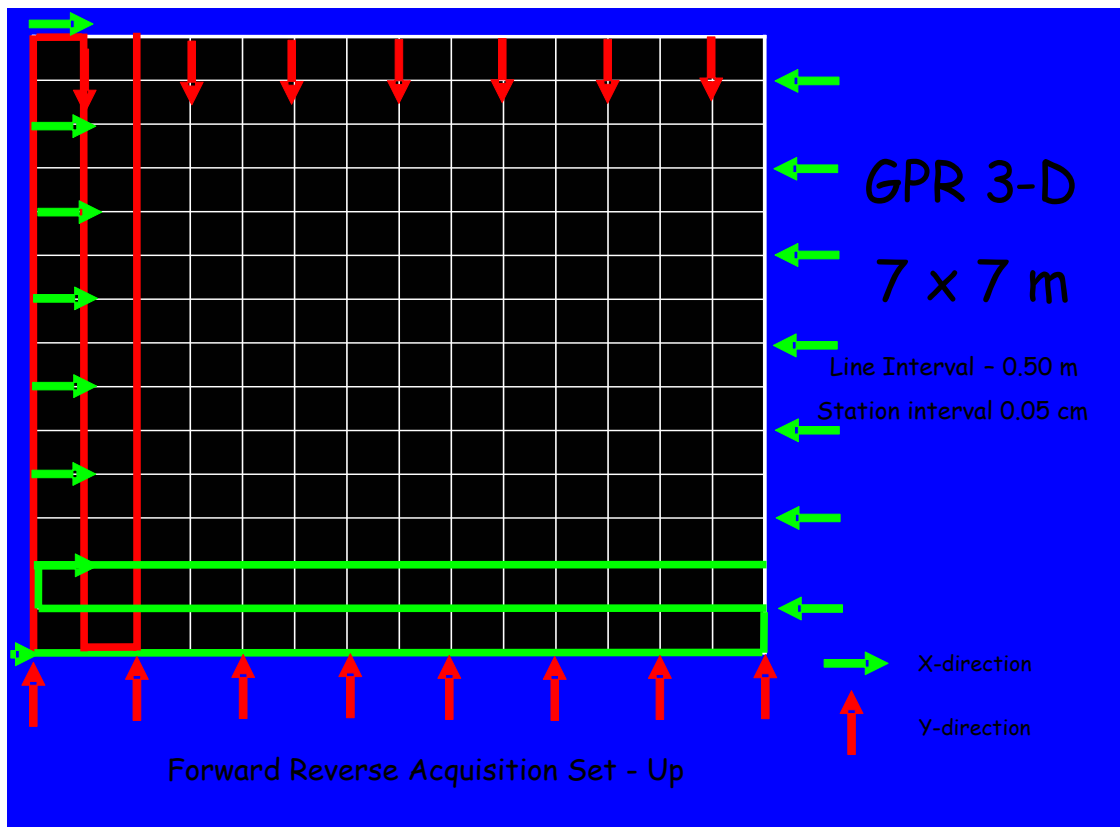
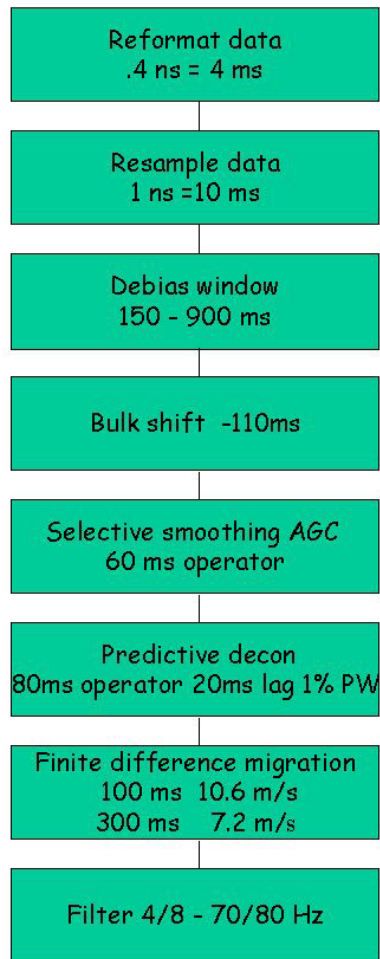


FIG. 4 3-D GPR acquisition methodology at plaza.

FIG. 5 GPR Processing Flow



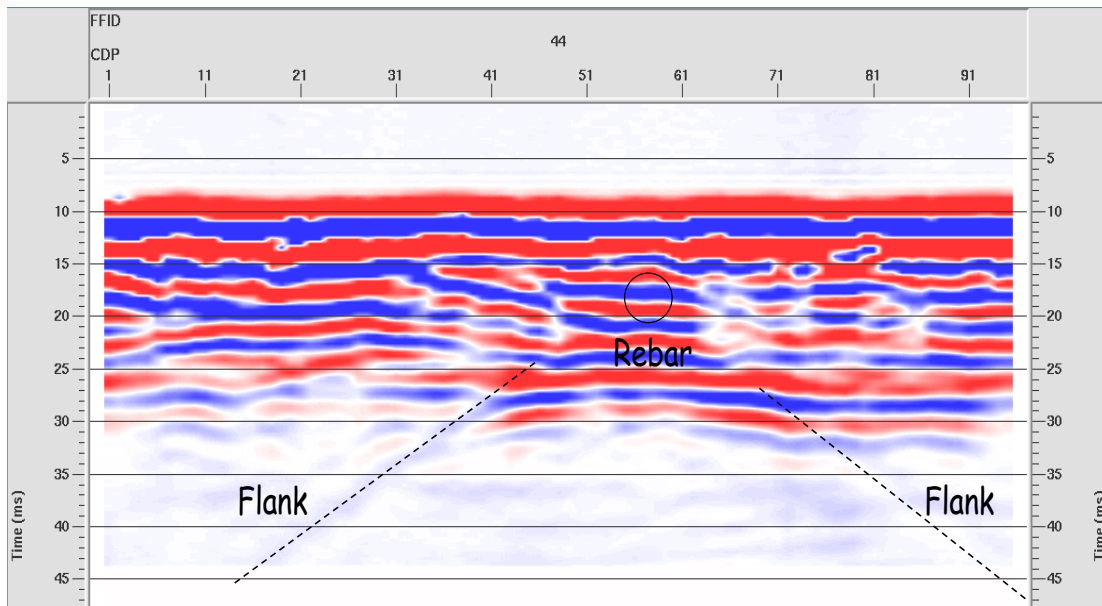


FIG.6 Filtered AGC stack of rebar line acquired adjacent to the excavated pit. Note the strong diffraction off the rebar at CDP 58.

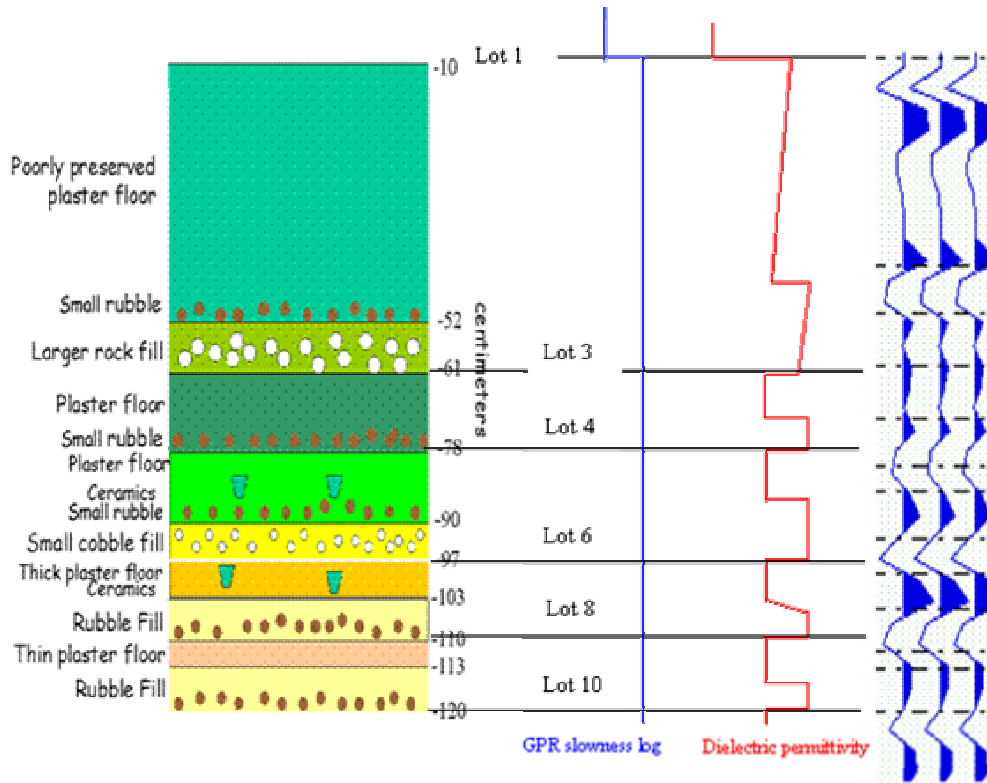


FIG. 7 Archaeological information from the excavated pit. A pseudo-radar slowness log (blue), a pseudo dielectric permittivity log (red) and a synthetic radargram are aligned for comparison.

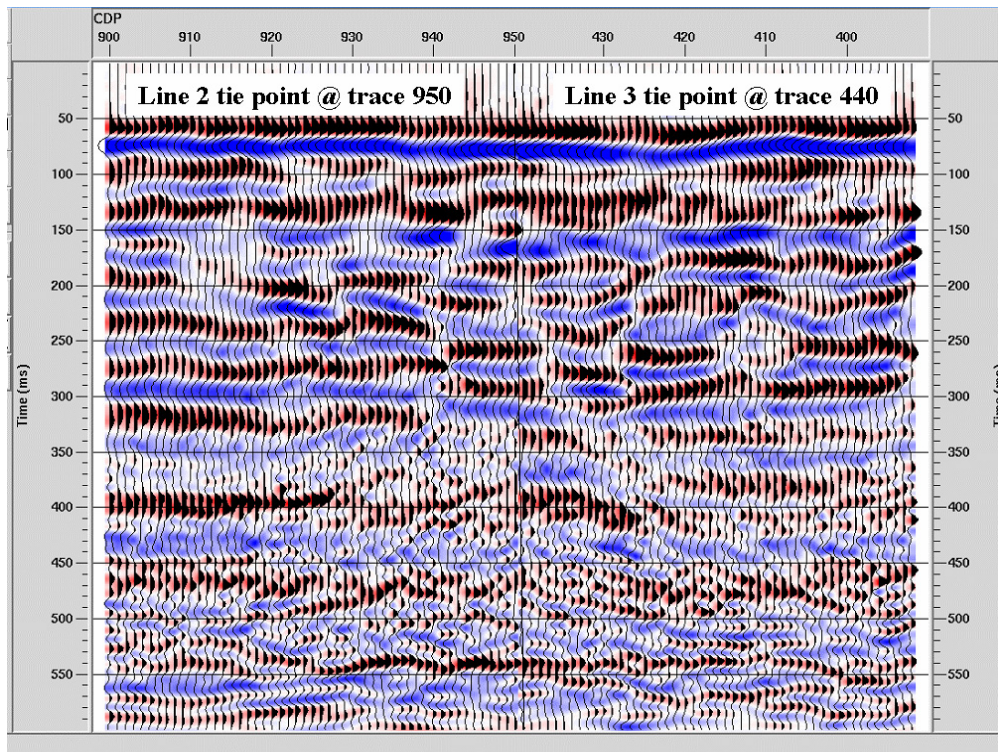


FIG. 8 Comparison of tie points between GPR lines.

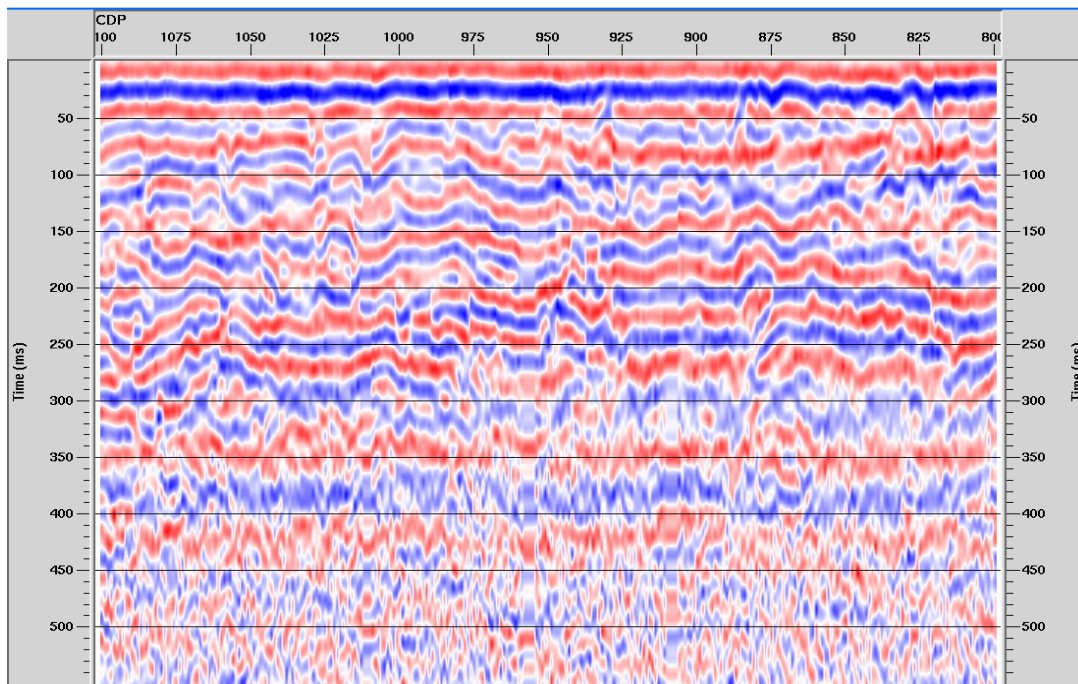


FIG. 9 Filtered stack of N-S Plaza Line 2.

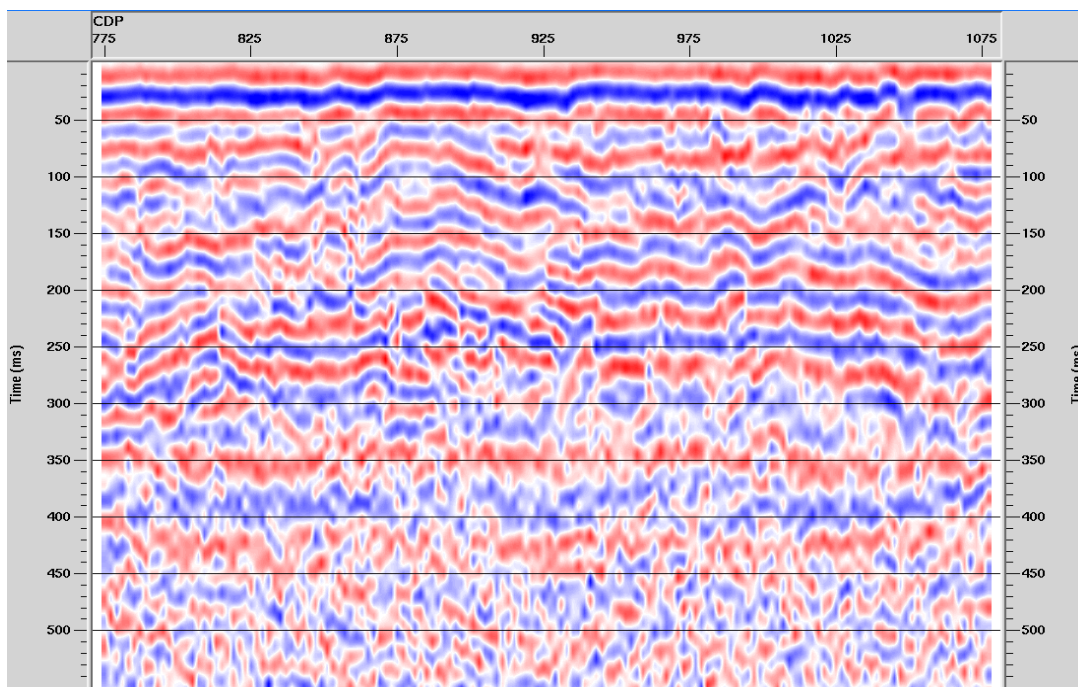


FIG. 10 Filtered stack of Project 3 Line 2 which is the reverse direction to the above figure.

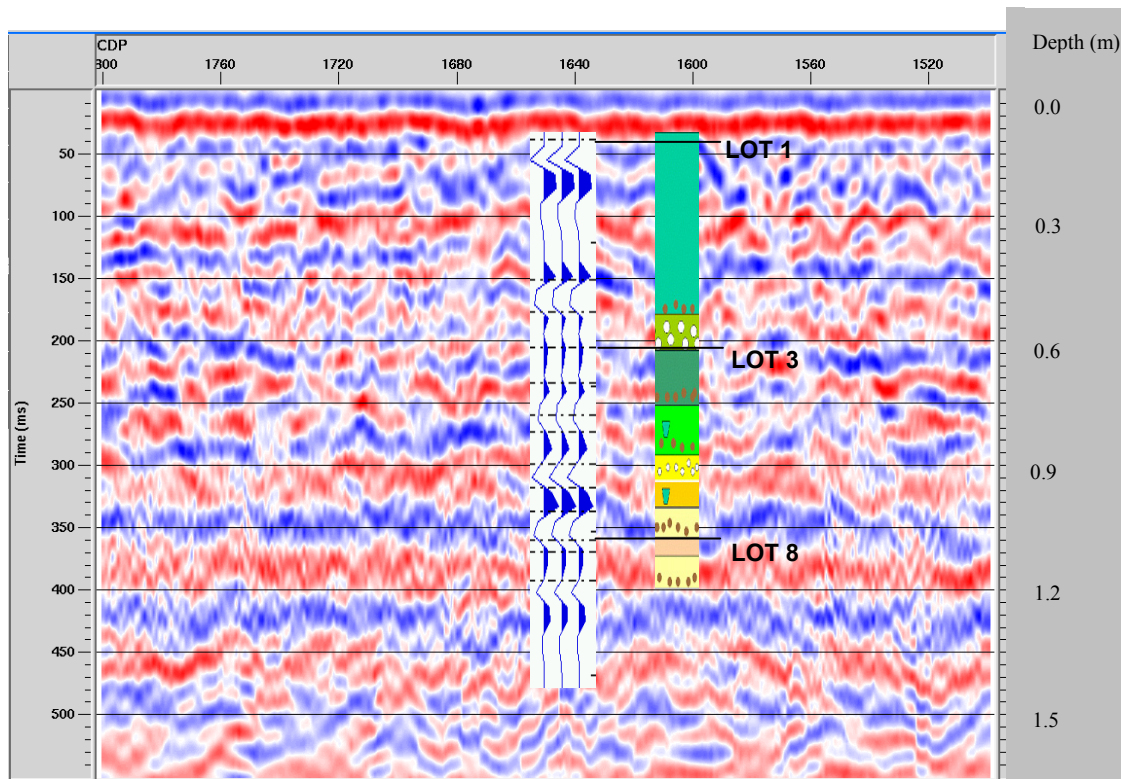


FIG. 11 Filtered, deconvolved, and migrated stack of N-S Plaza Line 2. The GPR radargram and archaeological pit have been superimposed and tied to the GPR section.

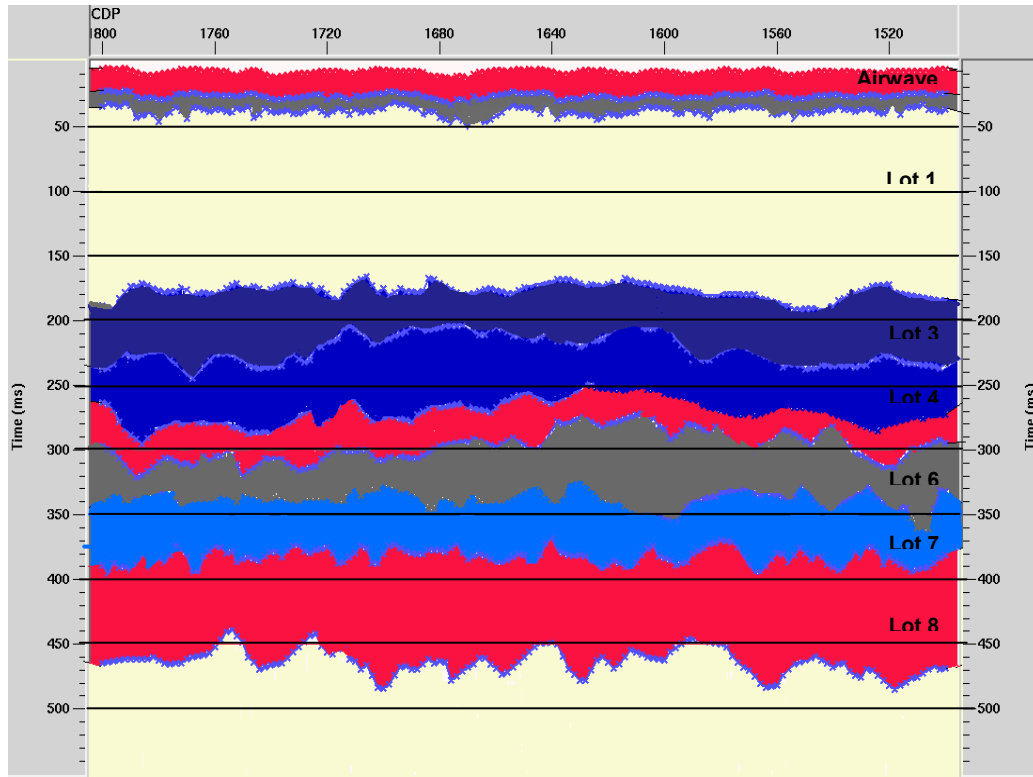


FIG. 12 The interpretation of the individual layers or lot numbers from the archaeological pit. Note the choppiness of the layering due to the scattering of electromagnetic energy from the rock fill and rubble.

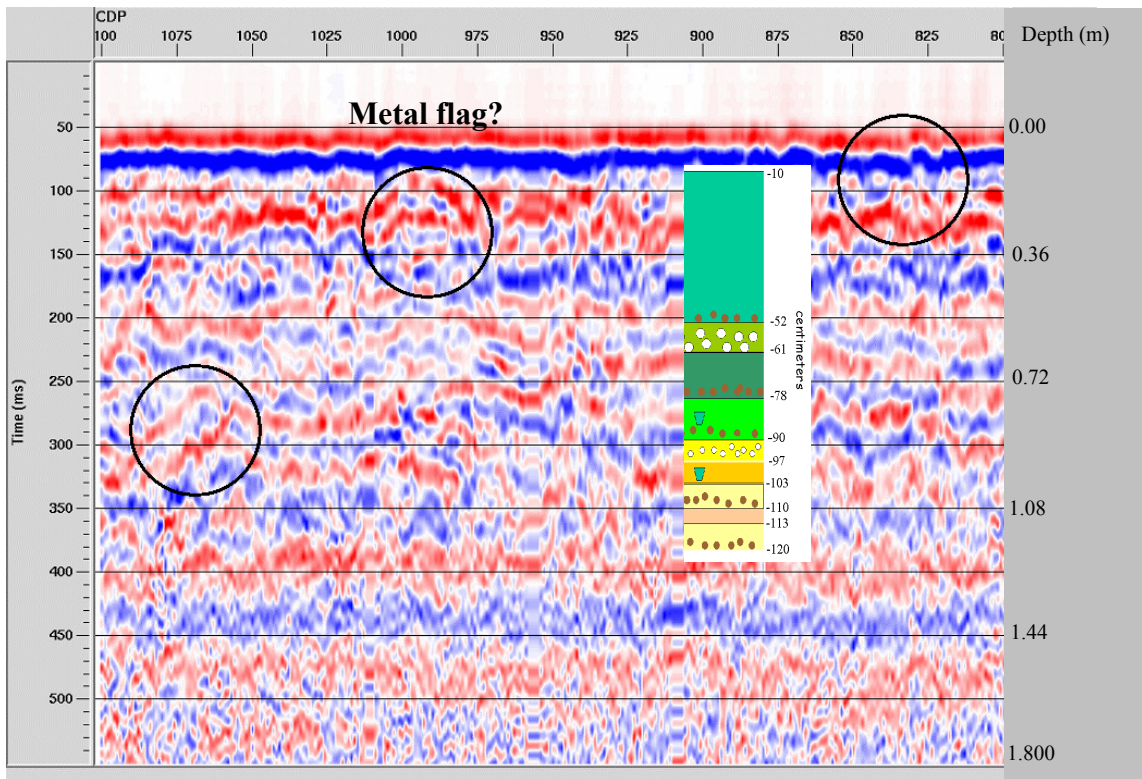


FIG. 13 Filtered deconvolved stack of Plaza Line 2. Black circles highlight several anomalies.

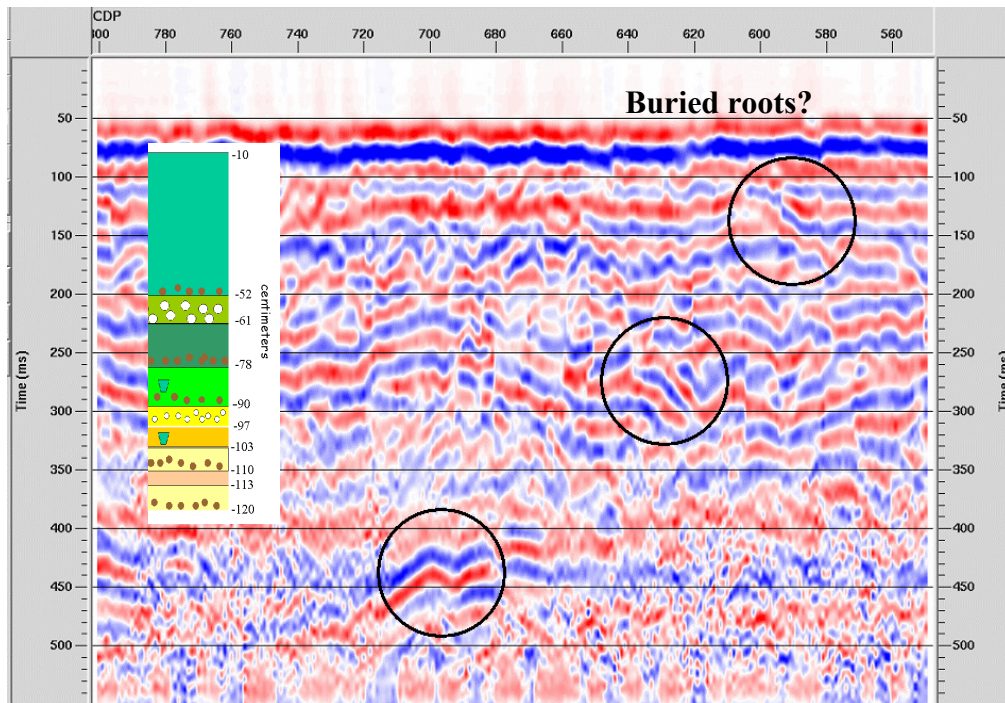


FIG. 14 Filtered stack of E-W Plaza Line 1. Black circles highlight several anomalies.

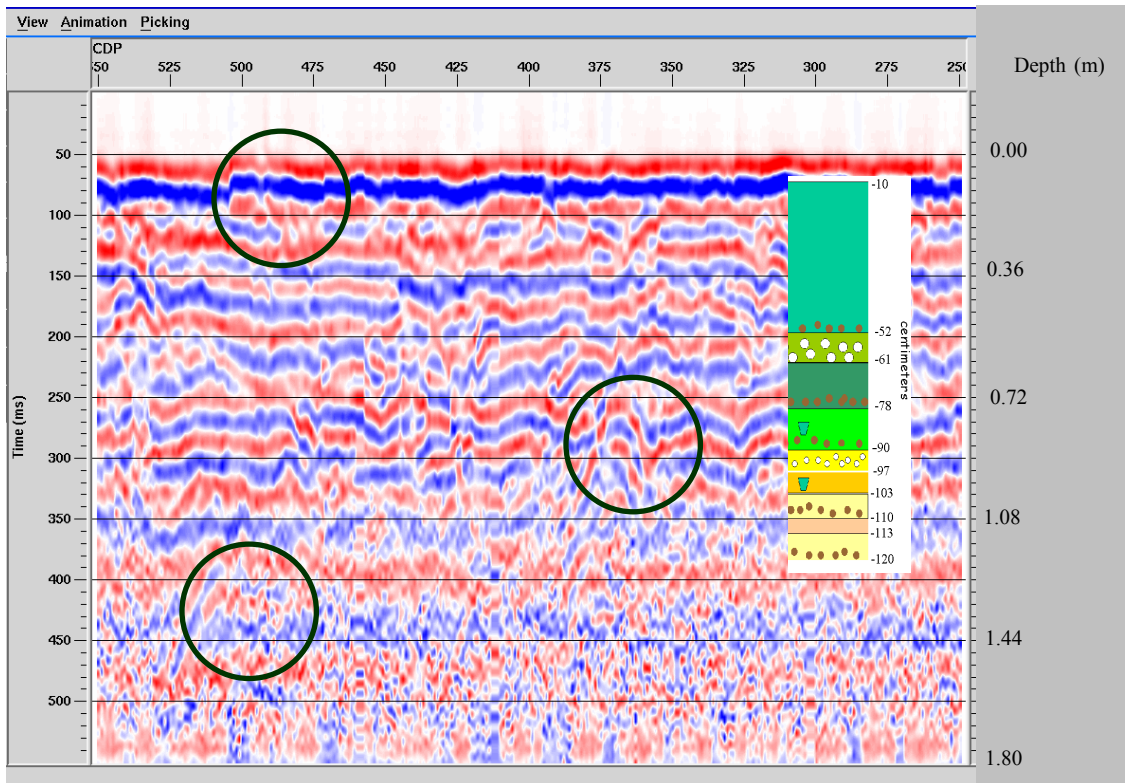


FIG. 15 Filtered stack of E-W Plaza Line 3. Black circles highlight several anomalies.

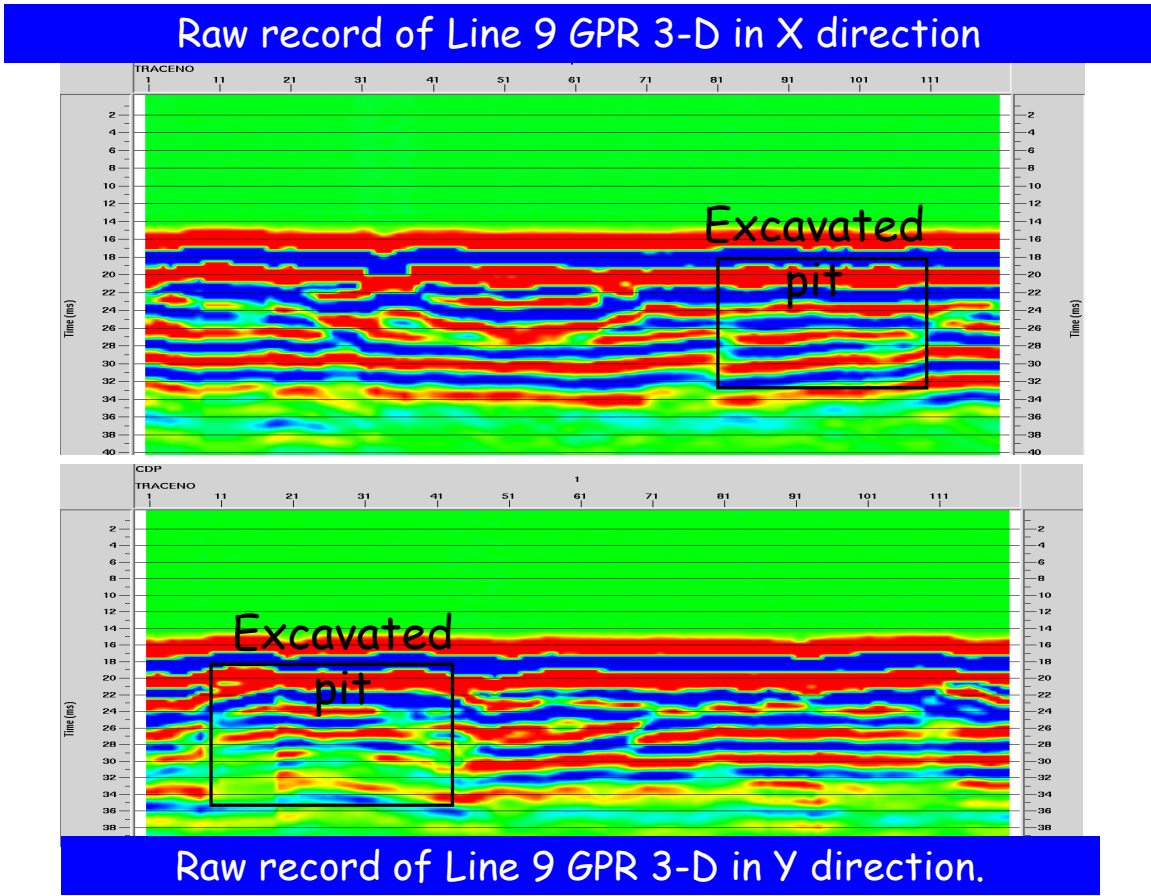


FIG.16 Raw records of the lines acquired across the excavated pit.

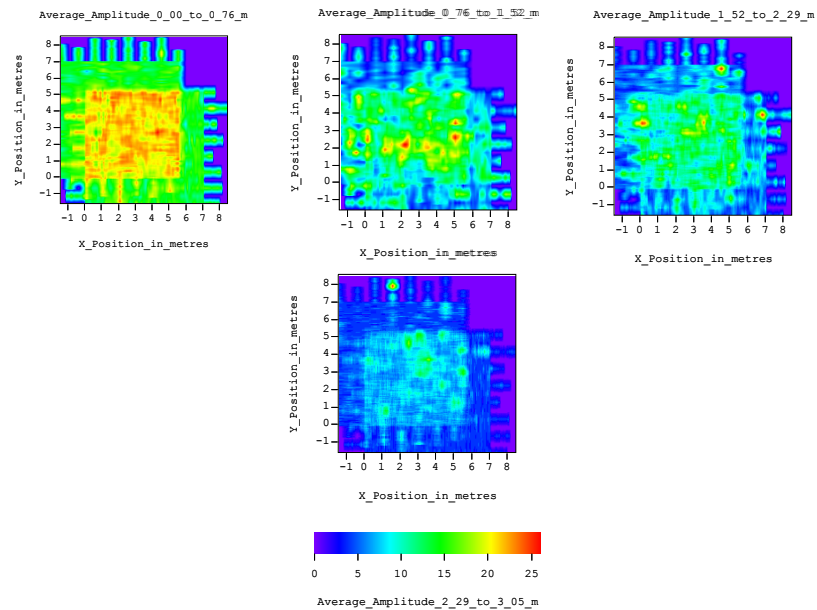


FIG. 17 Time slices through GPR data volume highlighting amplitude anomalies.

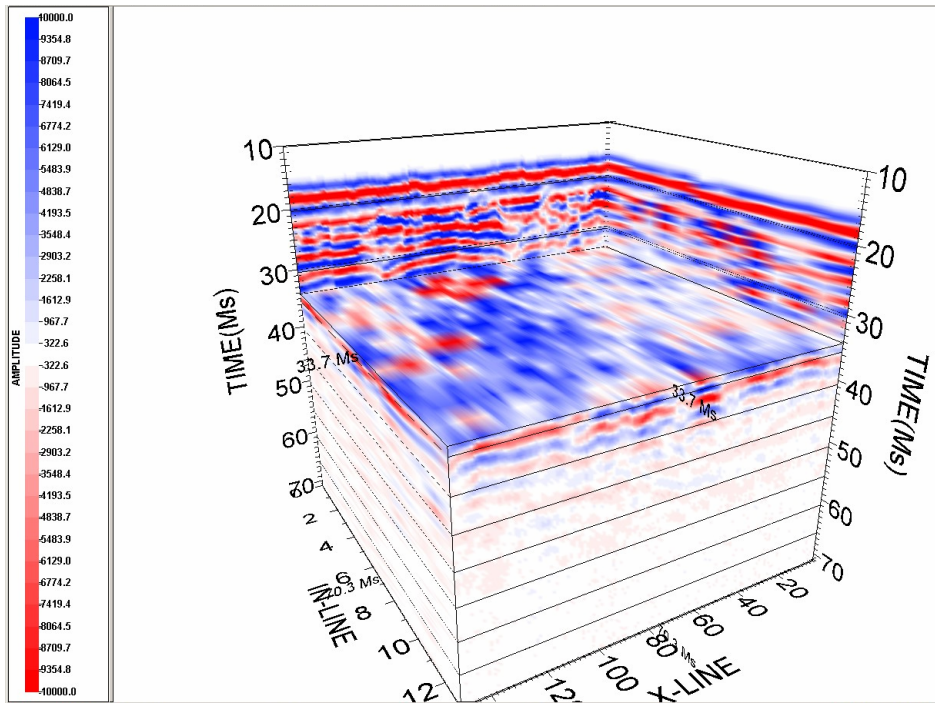


FIG. 18 3-D Grid from the plaza in the X or inline direction.

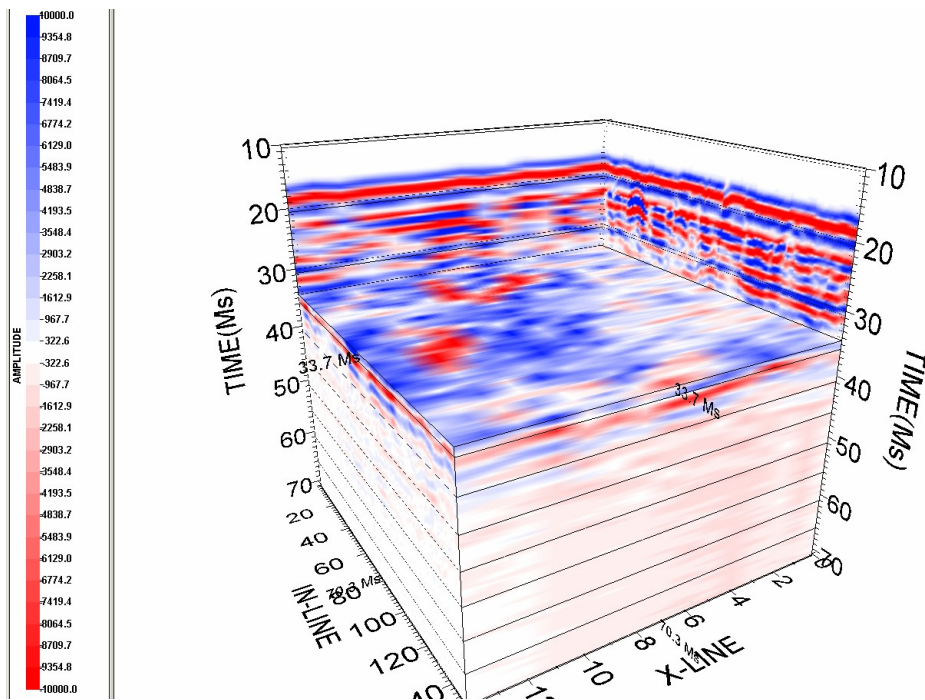


FIG. 19 3-D grid from the plaza in the Y or crossline direction.